

Measurement of the angle ϕ_3 with Dalitz analysis of three-body D^0 decay from $B \rightarrow D^0 K$ process

K. Abe,⁹ K. Abe,⁴⁴ N. Abe,⁴⁷ R. Abe,³⁰ T. Abe,⁹ I. Adachi,⁹ Byoung Sup Ahn,¹⁶
H. Aihara,⁴⁶ M. Akatsu,²³ M. Asai,¹⁰ Y. Asano,⁵¹ T. Aso,⁵⁰ V. Aulchenko,² T. Aushev,¹³
S. Bahinipati,⁵ A. M. Bakich,⁴¹ Y. Ban,³⁴ E. Banas,²⁸ S. Banerjee,⁴² A. Bay,¹⁹ I. Bedny,²
P. K. Behera,⁵² I. Bizjak,¹⁴ A. Bondar,² A. Bozek,²⁸ M. Bračko,^{21,14} J. Brodzicka,²⁸
T. E. Browder,⁸ M.-C. Chang,²⁷ P. Chang,²⁷ Y. Chao,²⁷ K.-F. Chen,²⁷ B. G. Cheon,⁴⁰
R. Chistov,¹³ S.-K. Choi,⁷ Y. Choi,⁴⁰ Y. K. Choi,⁴⁰ M. Danilov,¹³ M. Dash,⁵³
E. A. Dodson,⁸ L. Y. Dong,¹¹ R. Dowd,²² J. Dragic,²² A. Drutskoy,¹³ S. Eidelman,²
V. Eiges,¹³ Y. Enari,²³ D. Epifanov,² C. W. Everton,²² F. Fang,⁸ H. Fujii,⁹ C. Fukunaga,⁴⁸
N. Gabyshev,⁹ A. Garmash,^{2,9} T. Gershon,⁹ G. Gokhroo,⁴² B. Golob,^{20,14} A. Gordon,²²
M. Grosse Perdekamp,³⁶ H. Guler,⁸ R. Guo,²⁵ J. Haba,⁹ C. Hagner,⁵³ F. Handa,⁴⁵
K. Hara,³² T. Hara,³² Y. Harada,³⁰ N. C. Hastings,⁹ K. Hasuko,³⁶ H. Hayashii,²⁴
M. Hazumi,⁹ E. M. Heenan,²² I. Higuchi,⁴⁵ T. Higuchi,⁹ L. Hinz,¹⁹ T. Hojo,³² T. Hokuue,²³
Y. Hoshi,⁴⁴ K. Hoshina,⁴⁹ W.-S. Hou,²⁷ Y. B. Hsiung,^{27,*} H.-C. Huang,²⁷ T. Igaki,²³
Y. Igarashi,⁹ T. Iijima,²³ K. Inami,²³ A. Ishikawa,²³ H. Ishino,⁴⁷ R. Itoh,⁹ M. Iwamoto,³
H. Iwasaki,⁹ M. Iwasaki,⁴⁶ Y. Iwasaki,⁹ H. K. Jang,³⁹ R. Kagan,¹³ H. Kakuno,⁴⁷
J. Kaneko,⁴⁷ J. H. Kang,⁵⁵ J. S. Kang,¹⁶ P. Kapusta,²⁸ M. Kataoka,²⁴ S. U. Kataoka,²⁴
N. Katayama,⁹ H. Kawai,³ H. Kawai,⁴⁶ Y. Kawakami,²³ N. Kawamura,¹ T. Kawasaki,³⁰
N. Kent,⁸ A. Kibayashi,⁴⁷ H. Kichimi,⁹ D. W. Kim,⁴⁰ Heejong Kim,⁵⁵ H. J. Kim,⁵⁵
H. O. Kim,⁴⁰ Hyunwoo Kim,¹⁶ J. H. Kim,⁴⁰ S. K. Kim,³⁹ T. H. Kim,⁵⁵ K. Kinoshita,⁵
S. Kobayashi,³⁷ P. Koppenburg,⁹ K. Korotushenko,³⁵ S. Korpar,^{21,14} P. Križan,^{20,14}
P. Krokovny,² R. Kulasiri,⁵ S. Kumar,³³ E. Kurihara,³ A. Kusaka,⁴⁶ A. Kuzmin,²
Y.-J. Kwon,⁵⁵ J. S. Lange,^{6,36} G. Leder,¹² S. H. Lee,³⁹ T. Lesiak,²⁸ J. Li,³⁸ A. Limosani,²²
S.-W. Lin,²⁷ D. Liventsev,¹³ R.-S. Lu,²⁷ J. MacNaughton,¹² G. Majumder,⁴² F. Mandl,¹²
D. Marlow,³⁵ T. Matsubara,⁴⁶ T. Matsuishi,²³ H. Matsumoto,³⁰ S. Matsumoto,⁴
T. Matsumoto,⁴⁸ A. Matyja,²⁸ Y. Mikami,⁴⁵ W. Mitaroff,¹² K. Miyabayashi,²⁴
Y. Miyabayashi,²³ H. Miyake,³² H. Miyata,³⁰ L. C. Moffitt,²² D. Mohapatra,⁵³
G. R. Moloney,²² G. F. Moorhead,²² S. Mori,⁵¹ T. Mori,⁴⁷ J. Mueller,^{9,†} A. Murakami,³⁷
T. Nagamine,⁴⁵ Y. Nagasaka,¹⁰ T. Nakadaira,⁴⁶ E. Nakano,³¹ M. Nakao,⁹ H. Nakazawa,⁹
J. W. Nam,⁴⁰ S. Narita,⁴⁵ Z. Natkaniec,²⁸ K. Neichi,⁴⁴ S. Nishida,⁹ O. Nitoh,⁴⁹
S. Noguchi,²⁴ T. Nozaki,⁹ A. Ogawa,³⁶ S. Ogawa,⁴³ F. Ohno,⁴⁷ T. Ohshima,²³ T. Okabe,²³
S. Okuno,¹⁵ S. L. Olsen,⁸ Y. Onuki,³⁰ W. Ostrowicz,²⁸ H. Ozaki,⁹ P. Pakhlov,¹³ H. Palka,²⁸
C. W. Park,¹⁶ H. Park,¹⁸ K. S. Park,⁴⁰ N. Parslow,⁴¹ L. S. Peak,⁴¹ M. Pernicka,¹²
J.-P. Perroud,¹⁹ M. Peters,⁸ L. E. Piilonen,⁵³ A. Polouektov,² F. J. Ronga,¹⁹ N. Root,²
M. Rozanska,²⁸ H. Sagawa,⁹ S. Saitoh,⁹ Y. Sakai,⁹ H. Sakamoto,¹⁷ H. Sakaue,³¹
T. R. Sarangi,⁵² M. Satpathy,⁵² A. Satpathy,^{9,5} O. Schneider,¹⁹ S. Schrenk,⁵
J. Schümann,²⁷ C. Schwanda,^{9,12} A. J. Schwartz,⁵ T. Seki,⁴⁸ S. Semenov,¹³ K. Senyo,²³
Y. Settai,⁴ R. Seuster,⁸ M. E. Sevir,²² T. Shibata,³⁰ H. Shibuya,⁴³ M. Shimoyama,²⁴
B. Shwartz,² V. Sidorov,² V. Siegle,³⁶ J. B. Singh,³³ N. Soni,³³ S. Stanič,^{51,‡} M. Starič,¹⁴
A. Sugi,²³ A. Sugiyama,³⁷ K. Sumisawa,⁹ T. Sumiyoshi,⁴⁸ K. Suzuki,⁹ S. Suzuki,⁵⁴
S. Y. Suzuki,⁹ S. K. Swain,⁸ K. Takahashi,⁴⁷ F. Takasaki,⁹ B. Takeshita,³² K. Tamai,⁹
Y. Tamai,³² N. Tamura,³⁰ K. Tanabe,⁴⁶ J. Tanaka,⁴⁶ M. Tanaka,⁹ G. N. Taylor,²²

A. Tchouvikov,³⁵ Y. Teramoto,³¹ S. Tokuda,²³ M. Tomoto,⁹ T. Tomura,⁴⁶ S. N. Tovey,²²
 K. Trabelsi,⁸ T. Tsuboyama,⁹ T. Tsukamoto,⁹ K. Uchida,⁸ S. Uehara,⁹ K. Ueno,²⁷
 T. Uglov,¹³ Y. Unno,³ S. Uno,⁹ N. Uozaki,⁴⁶ Y. Ushiroda,⁹ S. E. Vahsen,³⁵ G. Varner,⁸
 K. E. Varvell,⁴¹ C. C. Wang,²⁷ C. H. Wang,²⁶ J. G. Wang,⁵³ M.-Z. Wang,²⁷
 M. Watanabe,³⁰ Y. Watanabe,⁴⁷ L. Widhalm,¹² E. Won,¹⁶ B. D. Yabsley,⁵³ Y. Yamada,⁹
 A. Yamaguchi,⁴⁵ H. Yamamoto,⁴⁵ T. Yamanaka,³² Y. Yamashita,²⁹ Y. Yamashita,⁴⁶
 M. Yamauchi,⁹ H. Yanai,³⁰ Heyoung Yang,³⁹ J. Yashima,⁹ P. Yeh,²⁷ M. Yokoyama,⁴⁶
 K. Yoshida,²³ Y. Yuan,¹¹ Y. Yusa,⁴⁵ H. Yuta,¹ C. C. Zhang,¹¹ J. Zhang,⁵¹ Z. P. Zhang,³⁸
 Y. Zheng,⁸ V. Zhilich,² Z. M. Zhu,³⁴ T. Ziegler,³⁵ D. Žontar,^{20,14} and D. Zürcher¹⁹

(The Belle Collaboration)

¹*Aomori University, Aomori*

²*Budker Institute of Nuclear Physics, Novosibirsk*

³*Chiba University, Chiba*

⁴*Chuo University, Tokyo*

⁵*University of Cincinnati, Cincinnati, Ohio 45221*

⁶*University of Frankfurt, Frankfurt*

⁷*Gyeongsang National University, Chinju*

⁸*University of Hawaii, Honolulu, Hawaii 96822*

⁹*High Energy Accelerator Research Organization (KEK), Tsukuba*

¹⁰*Hiroshima Institute of Technology, Hiroshima*

¹¹*Institute of High Energy Physics,*

Chinese Academy of Sciences, Beijing

¹²*Institute of High Energy Physics, Vienna*

¹³*Institute for Theoretical and Experimental Physics, Moscow*

¹⁴*J. Stefan Institute, Ljubljana*

¹⁵*Kanagawa University, Yokohama*

¹⁶*Korea University, Seoul*

¹⁷*Kyoto University, Kyoto*

¹⁸*Kyungpook National University, Taegu*

¹⁹*Institut de Physique des Hautes Énergies, Université de Lausanne, Lausanne*

²⁰*University of Ljubljana, Ljubljana*

²¹*University of Maribor, Maribor*

²²*University of Melbourne, Victoria*

²³*Nagoya University, Nagoya*

²⁴*Nara Women's University, Nara*

²⁵*National Kaohsiung Normal University, Kaohsiung*

²⁶*National Lien-Ho Institute of Technology, Miao Li*

²⁷*Department of Physics, National Taiwan University, Taipei*

²⁸*H. Niewodniczanski Institute of Nuclear Physics, Krakow*

²⁹*Nihon Dental College, Niigata*

³⁰*Niigata University, Niigata*

³¹*Osaka City University, Osaka*

³²*Osaka University, Osaka*

³³*Panjab University, Chandigarh*

³⁴*Peking University, Beijing*

³⁵*Princeton University, Princeton, New Jersey 08545*

³⁶*RIKEN BNL Research Center, Upton, New York 11973*

³⁷*Saga University, Saga*

³⁸*University of Science and Technology of China, Hefei*

³⁹*Seoul National University, Seoul*

⁴⁰*Sungkyunkwan University, Suwon*

⁴¹*University of Sydney, Sydney NSW*

⁴²*Tata Institute of Fundamental Research, Bombay*

⁴³*Toho University, Funabashi*

⁴⁴*Tohoku Gakuin University, Tagajo*

⁴⁵*Tohoku University, Sendai*

⁴⁶*Department of Physics, University of Tokyo, Tokyo*

⁴⁷*Tokyo Institute of Technology, Tokyo*

⁴⁸*Tokyo Metropolitan University, Tokyo*

⁴⁹*Tokyo University of Agriculture and Technology, Tokyo*

⁵⁰*Toyama National College of Maritime Technology, Toyama*

⁵¹*University of Tsukuba, Tsukuba*

⁵²*Utkal University, Bhubaneswer*

⁵³*Virginia Polytechnic Institute and State University, Blacksburg, Virginia 24061*

⁵⁴*Yokkaichi University, Yokkaichi*

⁵⁵*Yonsei University, Seoul*

(Dated: August 13, 2003)

Abstract

A new method to measure the angle ϕ_3 of the CKM unitarity triangle using a Dalitz analysis of the three-body decay of the D^0 meson from the $B \rightarrow D^0 K$ process has been introduced recently. The method employs the interference between D^0 and \bar{D}^0 to extract both the weak and strong phases. We present a study of statistical and systematic errors of this method using Monte Carlo simulation. A fit of the D^0 Dalitz distribution has been performed based on a 140 fb^{-1} sample collected by the Belle detector. We observe the indication of a CP asymmetry with the significance of 2.4 standard deviations. The 90% confidence interval obtained for the ϕ_3 value is $61^\circ < \phi_3 < 142^\circ$.

PACS numbers: 11.30.Er, 12.15.Hh, 13.25.Hw

INTRODUCTION

The determination of the Cabibbo-Kobayashi-Maskawa (CKM) matrix elements [1] is important to check the consistency of the Standard Model and search for new physics. Various methods using $B \rightarrow DK$ decays have been introduced [2] to measure the unitarity triangle angle ϕ_3 but these require knowledge of the branching fractions for different $B \rightarrow DK$ modes and therefore suffer from systematic errors due to detector response and background contamination.

A novel technique based on the analysis of the three-body decay of the D^0 meson [3] does not involve absolute branching fraction measurements and is, therefore, free from corresponding detector systematics. At the same time, the uncertainties in this method due to the D^0 decay model can be controlled.

This method is based on two key observations: neutral D^0 and \bar{D}^0 mesons can decay to a common final state such as $K_S\pi^+\pi^-$, and the decay $B \rightarrow D^0K^{(*)}$ can produce neutral D^0 mesons of both flavors via $b \rightarrow c\bar{u}s$ and $b \rightarrow u\bar{c}s$ transitions (see Figure 1), where the relative phase between the two interfering amplitudes is the sum $\delta + \phi_3$ of strong and weak interaction phases. In the charge conjugate mode, the relative phase is the difference $\delta - \phi_3$ of these phases, so both phases can be extracted from the measurements of such B decays and their charge conjugate modes. The annihilation diagram contribution is neglected here since it affects only the extracted value of the strong phase δ . In our case, the measurement is based on the analysis of Dalitz distribution of the three body final state of the $D^{(*)}$ meson.

In this paper, we will discuss in detail the decay $B^+ \rightarrow \bar{D}^0K^+$ state only, although a similar approach can be applied to other processes such as $B^0 \rightarrow D^0K^{*0}$ or $B^\pm \rightarrow D^{*0}K^\pm$.

DESCRIPTION OF THE METHOD

In the Wolfenstein parameterization of the CKM matrix, the amplitudes of the two diagrams shown in Fig. 1 that contribute to the decay $B^+ \rightarrow D^0(\bar{D}^0)K^+$ are given by $M_1 \sim V_{cb}V_{us}^* \sim A\lambda^3$ and $M_2 \sim V_{ub}V_{cs}^* \sim A\lambda^3(\rho + i\eta)$. These amplitudes interfere if the D^0 and \bar{D}^0 mesons decay into the identical final state $K_S\pi^+\pi^-$; we denote the admixed state as \tilde{D}^0 . Assuming no CP asymmetry in D^0 decays, the amplitude of the B^+ decay can be written as

$$M_+ = f(m_+^2, m_-^2) + ae^{i\phi_3+i\delta}f(m_-^2, m_+^2), \quad (1)$$

where m_+^2 and m_-^2 are the squared invariant masses of the $K_S\pi^+$ and $K_S\pi^-$ combinations, respectively, and f is the complex amplitude of the decay $\tilde{D}^0 \rightarrow K_S\pi^+\pi^-$. The absolute value a of the ratio between the two interfering amplitudes is given by

$$a = \frac{|V_{ub}V_{cs}^*|}{|V_{cb}V_{us}^*|} \cdot \frac{|a_2|}{|a_1|} \sim 0.08 \cdot 1.04/0.2196 \cdot 0.35,$$

where the color suppression factor $|a_2/a_1|$ can be estimated from the Belle measurements of the color suppressed $\bar{B}^0 \rightarrow D^0\bar{K}^0$ [5] and color allowed $B^- \rightarrow D^0K^-$ [6] decays:

$$\frac{|a_2|}{|a_1|} = \sqrt{\frac{Br(\bar{B}^0 \rightarrow D^0\bar{K}^0)}{Br(B^- \rightarrow D^0K^-)}} = 0.35.$$

Though there are estimations of the a value as large as 0.2 [7], in our Monte Carlo (MC) simulations, we have used the conservative value of $a = 0.125$.

Similarly, the amplitude of the charge conjugate B^- decay is

$$M_- = f(m_-^2, m_+^2) + ae^{-i\phi_3+i\delta} f(m_+^2, m_-^2).$$

Once the functional form of f is fixed by a choice of a model for $D^0 \rightarrow K_s\pi^+\pi^-$ decays, the Dalitz distributions for B^+ and B^- decays can be fitted simultaneously by the above expressions for M_+ and M_- , with a , ϕ_3 , and δ as free parameters.

Ref. [3] suggests a model-independent way of determining ϕ_3 via a binned Dalitz plot analysis. However, this method is likely to introduce higher statistical errors in our present statistics-limited stage, and certain technical issues involving backgrounds and reconstruction efficiency have to be solved. Here, we use a model-dependent approach with an unbinned maximum likelihood fit of the Dalitz distribution, making optimal use of our small event sample.

STUDY OF SENSITIVITY AND MODEL UNCERTAINTIES

The accuracy of the ϕ_3 determination and possible systematic effects are determined from a MC simulation, where we generate a large number of $\bar{D}^0 \rightarrow K_s\pi^+\pi^-$ decays according to a selected model of the D^0 decay, then perform the unbinned likelihood fit of the Dalitz distribution to obtain the parameter values and their errors.

The Dalitz plot for the decay $B^+ \rightarrow [K_s\pi^+\pi^-]_{\bar{D}^0} K^+$ in the variables m_+^2 and m_-^2 was generated according to relation (1), with the $D^0 \rightarrow K_s\pi^+\pi^-$ decay amplitude f described by the set of resonances listed in Table I. The model used is similar to that in the CLEO measurement [8] except that tensors and $K^*(1680)$ are excluded. The amplitude f in this model is represented by a coherent sum of N two-body decay amplitudes plus one non-resonant decay amplitude:

$$f(m_+^2, m_-^2) = \sum_{j=1}^N a_j e^{i\alpha_j} A_j(m_+^2, m_-^2) + be^{i\beta},$$

where N is the number of resonances, $A_j(m_+^2, m_-^2)$, a_j and α_j are the matrix element, amplitude and phase, respectively, for the j -th resonance, and b and β are the amplitude and phase for the non-resonant component. The total phase and amplitude are arbitrary. To be consistent with CLEO, we have chosen the $K_s\rho$ mode to have unit amplitude and zero relative phase. The description of the matrix elements A_j follows Ref. [9].

The simulated Dalitz plot of the \bar{D}^0 decay is shown in Fig. 2. The corresponding distribution for the admixed \bar{D}^0 decay contains the information about the interference phase and amplitude between D^0 and \bar{D}^0 that can be extracted from the fit to the Dalitz distribution.

Though in general the whole Dalitz plot is sensitive to the variations of the phase between D^0 and \bar{D}^0 , the contribution from the interference is particularly high in certain regions. Since the maximum of the \bar{D}^0 plot density is in the region of $K^*(892)^+$, the most sensitive area is the region of double Cabibbo suppressed $K^*(892)^-$, which interferes with the maximum amplitude of color suppressed D^0 . Another sensitive part is the region of $K_s\rho$. Fig. 4 demonstrates the CP asymmetry on the most sensitive regions of the Dalitz distribution.

For the estimation of the statistical error of ϕ_3 , samples of 10^4 events were generated with total phase θ varying from 0 to 2π ($\theta = \delta + \phi_3$ for $B^+ \rightarrow \bar{D}^0 K^+$ and $\theta = \delta - \phi_3$ for $B^- \rightarrow D^0 K^-$ decay) and the resulting \bar{D}^0 distributions were fitted with a and θ as free

parameters. This is equivalent to the case where both B^+ and B^- decays are fitted with (a_+, θ_+) and (a_-, θ_-) as free parameters and the weak phase ϕ_3 is extracted as

$$\phi_3 = \frac{\theta_+ - \theta_-}{2}.$$

The error of ϕ_3 is slightly overestimated in this case since we do not constrain the relative amplitudes a_+ and a_- to be equal.

The error of ϕ_3 was determined as

$$\sigma_{\phi_3}^2(\phi_3, \delta) = \frac{1}{4}(\sigma_{\theta}^2(\delta + \phi_3) + \sigma_{\theta}^2(\delta - \phi_3)), \quad (2)$$

where σ_{θ} is the error of the parameter θ extracted from the fit. The corresponding statistical error σ_{ϕ_3} obtained with relation (2) ranges from 3.0° to 3.7° with a mean value of 3.4° (averaged over all ϕ_3 and δ).

We expect about 10^3 $B^+ \rightarrow [K_s \pi^+ \pi^-]_{\bar{D}^0} K^+$ decays from a 1000 fb^{-1} sample will result in a 10° statistical accuracy in ϕ_3 . The statistics of B decays collected at the present time by B -factories is therefore insufficient to make a ϕ_3 measurement with a reasonable precision. However, the 140 fb^{-1} sample of Belle could provide the evidence of a CP asymmetry.

We expect the model used for the $\bar{D}^0 \rightarrow K_s \pi^+ \pi^-$ decay to be one of the main sources of systematic errors of ϕ_3 . We estimate this contribution by fitting our simulated samples, described earlier, to five alternate models for the decay amplitude $f(m_+^2, m_-^2)$ (see Table II). It can be seen that while Blatt-Weisskopf form factors and q^2 resonance width dependence have a rather small effect on the model error, the exclusion of wide resonances and doubly Cabibbo suppressed $K^*(892)$ causes a large bias of ϕ_3 . We take the value of 10° as a rough estimate of the model uncertainty for the method. This value was obtained by taking only the narrow resonances (including doubly Cabibbo suppressed $K^*(892)$) and approximating the others with a flat non-resonant term. This is motivated by the fact that the amplitude of the narrow resonances is well approximated with a Breit-Wigner shape, whereas wide states ($\Gamma \sim M$) contain substantial theoretical uncertainties.

Though doubly Cabibbo suppressed $K^*(892)$ has a small amplitude compared to other resonances (its fit fraction is 0.34% [4]), the error in its amplitude transforms into a large systematic error since the whole area of the resonance interferes with the Cabibbo allowed $K^*(892)$ component of the color suppressed amplitude. We have investigated this influence by generating a sample of 10^4 events according to the model of Table I with subsequent fitting of this Dalitz plot with the same model where the amplitude of doubly Cabibbo suppressed $K^*(892)$ is changed. This analysis indicates that the statistical error of 0.02 on the $K^*(892)$ amplitude obtained by CLEO [8] transforms into approximately 3° bias in ϕ_3 . The errors of other amplitudes are expected to contribute even less, since they lie mainly outside the maximum sensitivity region of the Dalitz distribution.

Another source of systematics comes from various kinds of background. We expect three main background contributions to affect the determination of ϕ_3 :

- Background uniformly distributed over the Dalitz plot (combinatorial background),
- Background from $B^\pm \rightarrow D^0(\bar{D}^0)\pi^\pm$ events with a pion misidentified as a kaon (pion background),
- Background from $B^\pm \rightarrow D^0(\bar{D}^0)K^\pm$ events with a wrongly associated kaon of opposite sign (“wrong tag” background).

To consider the worst case scenario, our MC samples were generated with one or another of these backgrounds and then fit without any background component. Neglected combinatorial background at the level of 5% results in an 8° bias in ϕ_3 . Neglected $D\pi$ background, even at the level of 20%, does not induce an appreciable bias in ϕ_3 . The contribution of wrongly associated kaons, which tag the flavor of D^0 , has a larger effect on systematics, since half of such kaons have the wrong sign and such events will be misinterpreted as decays of a D meson of opposite flavor. These D^0 's will distort the most sensitive region of the Dalitz plot. According to our simulation, the 5% admixture of wrong tag background introduces a 12° bias of ϕ_3 .

DETERMINATION OF $D^0 \rightarrow K_s \pi \pi$ DECAY MODEL

For our MC simulation we have used the D^0 decay model measured by CLEO based on their data sample of 5300 events [8]. However, the integrated luminosity collected by Belle can offer a much bigger sample of D^0 events. We have analyzed 78 fb^{-1} of BELLE data looking for decays of $D^*(2010)^+ \rightarrow D^0 \pi^+$, $D^0 \rightarrow K_s \pi^+ \pi^-$ (and its charge conjugate). The selection was based on the D^0 candidate invariant mass ($|M_{K_s \pi \pi} - M_{D^0}| < 9 \text{ MeV}/c^2$), and the mass difference of the D^{*+} and D^0 candidates ($4.39 < \Delta M < 6.19 \text{ MeV}/c^2$). We require the CM momentum of the $D\pi$ system to be above $2.7 \text{ GeV}/c$ to avoid contamination from combinatorics of $b\bar{b}$ decays. We have selected 57800 events satisfying these requirements. The fit of the M_D distribution yields a background fraction of 5.6%.

The Dalitz plot for the selected $D^* \rightarrow D\pi \rightarrow (K_S \pi \pi)\pi$ candidates and its projections are shown in Fig. 3. The data were fitted with a list of resonances from the CLEO model plus two scalars (σ_1 and σ_2) in the $\pi\pi$ channel with free mass and width. We assumed the background and efficiency to be uniform over the allowed phase space. Our fit result is shown in Table III.

EVENT SELECTION

The Belle detector has been described in detail elsewhere [10]. It is a large-solid-angle magnetic spectrometer consisting of a three-layer silicon vertex detector (SVD), a 50-layer central drift chamber (CDC) for charged particle tracking and specific ionization measurement (dE/dx), an array of aerogel threshold Čerenkov counters (ACC), time-of-flight scintillation counters (TOF), and an array of 8736 CsI(Tl) crystals for electromagnetic calorimetry (ECL) located inside a superconducting solenoid coil that provides a 1.5 T magnetic field. An iron flux return located outside the coil is instrumented to detect K_L mesons and identify muons (KLM).

Separation of kaons and pions is accomplished by combining the responses of the ACC and the TOF with dE/dx measurement in the CDC to form a likelihood $\mathcal{L}(h)$ where h is a pion or a kaon. Charged particles are identified as pions or kaons using the likelihood ratio (PID):

$$\text{PID}(K) = \frac{\mathcal{L}(K)}{\mathcal{L}(K) + \mathcal{L}(\pi)}; \text{PID}(\pi) = \frac{\mathcal{L}(\pi)}{\mathcal{L}(K) + \mathcal{L}(\pi)} = 1 - \text{PID}(K).$$

The data sample of $152 \cdot 10^6 B\bar{B}$ events (140 fb^{-1}) collected by the Belle detector was processed to search for $B^\pm \rightarrow D^0 K^\pm$ decays with D^0 decaying into the $K_s \pi^+ \pi^-$ final state.

In addition, we select $B^\pm \rightarrow D^0\pi^\pm$ and $B^\pm \rightarrow D^*(2007)^0\pi^\pm$ decays which serve as test samples for our fitting procedure and are used for background analysis.

Neutral kaons are reconstructed from pairs of oppositely charged pions. We require the reconstructed vertex distance from the interaction point in the plane transverse to the beam axis to be more than 1 mm and the invariant mass $M_{\pi\pi}$ to be $|M_{\pi\pi} - M_{K_s}| < 10 \text{ MeV}/c^2$.

Selection of B candidates is based on the CM energy difference $\Delta E = \sum E_i - E_{beam}$ and B meson beam-constrained mass $M_{bc} = \sqrt{E_{beam}^2 - (\sum p_i)^2}$, where $E_{beam} = m_\Upsilon/2$ is the CM beam energy, and E_i and p_i are the CM energies and momenta of the B candidate decay products. We select events with $M_{bc} > 5.2 \text{ GeV}/c^2$ and $|\Delta E| < 0.2 \text{ GeV}$ for the analysis. The cuts for signal candidates are $5.272 < M_{bc} < 5.288 \text{ GeV}/c^2$ and $|\Delta E| < 0.022 \text{ GeV}$. In addition, we apply a cut on the invariant mass of the D^0 candidate: $|M_{K_s\pi\pi} - m_D| < 11 \text{ MeV}/c^2$.

To suppress the continuum background, we require $|\cos\theta_{thr}| < 0.8$, where θ_{thr} is the angle between the thrust axis of the B candidate and the rest of the event. For additional background rejection, we use the Fisher discriminant composed of 11 parameters [11]: the production angle of the B candidate, the angle of the B thrust axis relative to the beam axis and nine parameters representing the momentum flow in the event relative to the B thrust axis in the CM frame.

The selection efficiency for these cuts is 12%, based on MC simulation, implying an expectation of 158 ± 33 signal events in our data sample. The distributions for ΔE , M_{bc} and M_D for the experimental data are shown in Fig. 5. The number of $B \rightarrow D^0K$ events satisfying all selection criteria is 138.

To fit the M_{bc} distribution, we use the empirical background function suggested by the ARGUS collaboration [12] plus a Gaussian signal. The ΔE distribution is fit with a linear background plus two Gaussians representing the signal (with a mean value around zero) and background from $B \rightarrow D^0\pi$ with a pion misidentified as a kaon (with $\Delta E \sim 50 \text{ MeV}$). For the M_D fit we use a constant background plus a combination of two Gaussians for the signal. The resolutions of the parameters were extracted from the fit of $B \rightarrow D^0\pi$ data, described below.

The fit of the ΔE distribution yields 107 ± 12 signal events and 33 ± 3 background events, consistent with the expectation of 158 ± 33 signal events. The Dalitz plots of the selected candidates and their projections onto $M_{K_s\pi^+}^2$, $M_{K_s\pi^-}^2$ and $M_{\pi^+\pi^-}^2$ axes are shown separately for B^- and B^+ decays in Fig. 10 and Fig. 11, respectively. Note that for B^+ decays the axes are chosen so that the K^* band is aligned along the y -axis, as for B^- decays.

The $B^\pm \rightarrow D^0\pi^\pm$ selection cuts are the same as those for $B \rightarrow D^0K$, except that the cut on K/π PID probability is modified to select a pion ($Pr(K/\pi) > 0.5$). The same fit functions are used to fit ΔE , M_{bc} and M_D distributions as for $B \rightarrow D^0K$ (with only one Gaussian peak in ΔE), and the fitted distributions are shown in Fig. 6. The extracted resolutions of the selection parameters, used in the $B \rightarrow D^0K$ fits, are 13 MeV for ΔE , 3.2 MeV/ c^2 for M_{bc} and 6.3 MeV/ c^2 for M_D . The Dalitz distribution of the $D^0 \rightarrow K_s\pi^+\pi^-$ decay from $B \rightarrow D^0\pi$ process is shown in Fig. 7.

BACKGROUNDS

To fit the Dalitz plot correctly, backgrounds have to be taken into account in the fit model. For each of the background contributions, we need to obtain not only its fraction in the event sample, but also the Dalitz plot shape.

The largest contribution for the decay of our interest comes from the continuum $q\bar{q}$ background ($q = u, d, s, c$). It includes the background with purely combinatorial tracks, and continuum D^0 mesons combined with a random kaon. This type of background is analyzed using the off-resonant statistics collected below $\Upsilon(4S)$ as well as on-resonance data with $\cos\theta_{thr}$ and Fisher cuts applied to select continuum.

The background coming from $b\bar{b}$ events originates either from $B \rightarrow D^0K$ decay with some final state particles interchanged with combinatorial ones from the decay of the other B meson, or from other charged or neutral B decays (possibly with misidentified or lost particles). We subdivide the $b\bar{b}$ background into four types.

The $B \rightarrow D^0\pi$ process with a pion misidentified as a kaon is suppressed by the requirement on the K/π identification probability and CM energy difference. The fraction of this background is obtained by fitting the ΔE distribution; the Dalitz plot distribution is that of D^0 without the opposite flavor admixture.

Other decays of charged and neutral B mesons contributing to the background are investigated with a generic MC sample. Most surviving candidates are due to decay of one of the B mesons to the $D^{*0}X$ state, with some particles taken from the other B decay.

Events where one of the D^0 decay products is substituted by a combinatorial kaon or pion were studied using the MC data set where one of the B mesons from the $\Upsilon(4S)$ decays into the D^0K state.

Events where a valid D^0 is combined with a random flavor-tagging kaon are of importance, because half of the kaons have the wrong sign: such events will be misinterpreted as decays of \bar{D}^0 , thus introducing distortion in the most sensitive area of the Dalitz plot. This background was studied with the same MC sample as for D^0 combinatorics. No events of this kind were found, which allows us to put an upper limit of 0.4% (at 95% C. L.) on the fraction of this contribution.

The Dalitz plot shapes of all the backgrounds were parameterized with empirical functions that included polynomial terms as well as Breit-Wigner peaks. The investigation of the ΔE distribution for all considered backgrounds allows us to conclude that none of them except combinatorics in D^0 decay is peaked in ΔE . Therefore, a ΔE fit gives a good estimate of the total background rate, which is 23%. The fractions of each contribution are as follows: 14% for continuum combinatorics, 3% for D^0 from continuum, 0.5% for $B \rightarrow D^0\pi$, 4% for decays of B^\pm other than $B \rightarrow D^0K/\pi$, 2% for decays of neutral B and 0.4% for combinatorics in D^0 decay.

Another approach to take into account backgrounds is to use events from D^0 sidebands. Since all the backgrounds except D^0 from continuum and D^0 decay combinatorics are not peaked in the D^0 invariant mass distribution, the D^0 sidebands are a good approximation of the total background shape. The D^0 combinatoric background has a small fraction and can be neglected, and the shape of the continuum D^0 background is known and can be added separately. However, the statistics in $B \rightarrow D^0K$ decays is not sufficient to fit the background shape with good precision, so we use the $B \rightarrow D^0\pi$ sample for this purpose. This approach is used together with the flat background distribution to estimate the systematic uncertainty caused by our background parameterization.

FIT OF D^0 DALITZ PLOT

We use the unbinned likelihood technique to fit the Dalitz plot of both MC simulated and experimental samples. In the fit function of experimental data, finite momentum resolution

and efficiency were taken into account.

The value which is minimized in the fit is the inverse logarithm of the unbinned likelihood function

$$-2 \log L = -2 \left[\sum_{i=1}^n \log p(m_{i+}^2, m_{i-}^2) - \log \int_D p(m_+^2, m_-^2) dm_+^2 dm_-^2 \right],$$

where m_{i+}^2 , m_{i-}^2 are measured (or generated) Dalitz plot variables and $p(m_+^2, m_-^2)$ is the Dalitz plot density being fitted. The Dalitz plot density is a sum of the signal $D^0 - \bar{D}^0$ interference $|f(m_+^2, m_-^2) + ae^{-i\phi} f(m_-^2, m_+^2)|^2$ and the background distribution, convoluted with a momentum resolution function and multiplied by the efficiency shape. The efficiency and resolution functions were obtained with a MC simulation with D^0 decaying according to the phase space distribution.

To check the consistency of the ϕ_3 fit, the same fitting procedure was applied to $B \rightarrow D^{(*)0}\pi$ and $D^* \rightarrow D^0\pi$ test samples as well as the $B \rightarrow D^0K$ signal. The idea is to check the absence of opposite flavor amplitude a that can appear if the Dalitz plot shape is not described well by the fit model. In the case of $D^* \rightarrow D^0\pi$ data, we do not expect any contribution from opposite flavor (provided flavor tagging is correct), but this sample cannot serve as a good fit test since the same data are used to fit the D^0 decay model. So, these data can only indicate the defects of D^0 decay parameterization, which can affect the ϕ_3 fit. The sample of D^0 from $B \rightarrow D^{(*)0}\pi$ decay allows for a more reliable test of the fit procedure, since it is independent of the sample used to determine the model, and the background sources are expected to be similar to those for our signal. In the case of $B \rightarrow D^{(*)0}\pi$, however, a small opposite flavor amplitude is expected ($\sim |V_{ub}V_{cd}^*|/|V_{cb}V_{ud}^*|$) with $a \sim 0.01 - 0.02$.

For our ϕ_3 fit check, the free parameters for Dalitz plot fit were the relative amplitude a and total phase θ .

In the $D^* \rightarrow D^0\pi$ data fit, we have used the flat background with the same fraction as used in the case of determination of the D^0 model. The result of the fit is the following: $a = 0.0041 \pm 0.0050$, $\theta = 123^\circ \pm 62^\circ$ for D^0 decay and $a = 0.0047 \pm 0.0050$, $\theta = 114^\circ \pm 52^\circ$ for \bar{D}^0 decay, which is consistent with zero.

The fit results for $B \rightarrow D^0\pi$ are $a_- = 0.067 \pm 0.027$, $\theta_- = 228^\circ \pm 23^\circ$ for D^0 from $B^- \rightarrow D^0\pi^-$ decay and $a_+ = 0.065 \pm 0.029$, $\theta_+ = 232^\circ \pm 24^\circ$ for \bar{D}^0 from $B^+ \rightarrow D^0\pi^+$ decay. It should be noted that since the value of a is positive definite, the error of this parameter does not serve as a good measure of the $a = 0$ hypothesis. To demonstrate the deviation of the opposite flavor amplitude from zero, the real and imaginary parts of the complex relative amplitude $a \exp(-i\theta)$ are more suitable. Fig. 8 shows complex relative amplitude constraints for B^- and B^+ data separately. It can be seen from the plot that both amplitudes differ from the expected value by more than two standard deviations.

As another check of the consistency of our fit result with the $a = 0$ hypothesis, we have performed a toy MC study. A Dalitz plot of 1700 events (which corresponds to full statistics of $B \rightarrow D^0\pi$ with both flavors included) was generated in 566 trials with the model where $a = 0$, and the fit of these data was performed with a and ϕ allowed to float. The distribution of the parameter a for these trials is shown in Fig. 9. It can be seen from the plot that only $\sim 1\%$ of the a values are above 0.06. The bias observed needs further investigation. One of the possible reasons can be the variation of the background shape that is not parameterized by the fit function. Also, one cannot discount statistical fluctuation.

Another test sample of D^0 's with the small opposite flavor admixture is provided by the $B \rightarrow D^{*0}\pi$ decay with D^{*0} decaying into $D^0\pi^0$. The constraints on the complex amplitude are shown in Fig. 8 (right). In this case, we do not observe any significant opposite flavor amplitude. The result of the fit is $a_- = 0.057 \pm 0.054$, $\theta_- = 340 \pm 65$ for D^0 from $B^- \rightarrow D^{*0}\pi^-$ decay and $a_+ = 0.041 \pm 0.069$, $\theta_+ = 164 \pm 100$ for \bar{D}^0 from $B^+ \rightarrow D^{*0}\pi^+$. Though this sample is smaller (350 events) and it can not serve a reliable test of fit bias, we observe phases different from $B \rightarrow D^0\pi$ case, which can indicate that the fitting procedure itself does not introduce a bias to the phase.

For $D^0 - \bar{D}^0$ interference fit in $B \rightarrow D^0K$, we have performed a simultaneous fit with free parameters a , ϕ_3 and δ . The result of the fit overlaid on the experimental Dalitz distribution projections is shown in Fig. 10 and Fig. 11 for B^- and B^+ decays, respectively. The fit yields $a = 0.33 \pm 0.10$, $\phi_3 = 92^\circ \begin{smallmatrix} +19 \\ -17 \end{smallmatrix}$, $\delta = 165^\circ \begin{smallmatrix} +17 \\ -19 \end{smallmatrix}$. It should be noted that the fit errors are quite non-parabolic, since the phase error obtained from the fit is inversely proportional to the value of a . Therefore, the errors quoted can not reliably represent the accuracy of the measurement. The constraint plots on the pairs of parameters (ϕ_3, δ) and (a, ϕ_3) shown in Fig. 12 give more information about the accuracy and the statistical significance of the fit. The plots show one, two and three standard deviation contours of each pair of parameters. The central values are marked with crosses. For each of the plots, the third parameter was allowed to float.

Note the two-fold ambiguity of this method: (ϕ_3, δ) and $(\phi_3 + \pi, \delta + \pi)$ cannot be distinguished, as they lead to the same total phases. Since there are no reliable measurements or theoretical predictions of the value of the strong phase, we keep both values as solutions for our data.

The ϕ_3 statistical significance $-2 \log L/L_{max}$ is presented in Fig. 13 (left). The a and δ parameters were allowed to float.

To illustrate the observation of CP asymmetry and its significance, we have performed a separate fit of the B^+ and B^- data sets. The results of the fits are shown in Fig. 13 (right) as constraints on the complex relative amplitude $a \exp(i\theta)$, as in the case of test sample fits. The relative amplitude of the $B \rightarrow D^0\pi$ test sample fit is also shown for comparison. The asymmetry of three standard deviations is apparent.

The influence of the different sources of systematics on our fit result are presented in Table IV. The systematic error is dominated by the D^0 model uncertainty. The component related to the background parameterization was estimated by extracting the background shape from the M_D sidebands and by using the flat background distribution. As mentioned above, the efficiency shape and resolution were extracted from MC simulation. To estimate their contribution to the systematic error, we have used the flat efficiency and ‘‘ideal’’ resolution, respectively.

The nonzero opposite flavor amplitude we observe in the $B \rightarrow D^0\pi$ test sample may indicate some systematic effect such as background structure or a deficiency of the D^0 decay model. Since the source of this bias is indeterminate, we conservatively treat it as an additional systematic effect.

Since the relative amplitude a is positive definite, its fit value is biased towards the higher values by approximately one standard deviation. Consequently, the strong dependence of the ϕ_3 error on a can cause an overestimation of the ϕ_3 determination accuracy. However, the constraint plot of a vs. ϕ_3 (Fig. 12, right) shows no significant correlation between the parameters. Therefore, we have calculated the ϕ_3 and δ for the value of $a = 0.23$, which is one standard deviation lower than the value obtained in the fit. With model and systematic

errors taken into account, and a bias correction applied, our fit result can be presented as:

- Weak phase $\phi_3 = 95^\circ \begin{smallmatrix} +25 \\ -20 \end{smallmatrix} \pm 13^\circ \pm 10^\circ$,
- Strong phase $\delta = 162^\circ \begin{smallmatrix} +20 \\ -25 \end{smallmatrix} \pm 12^\circ \pm 24^\circ$.

The first error is statistical, the second is experimental systematics and the third is model uncertainty. Fig. 14 shows 90% CL regions for the pairs of parameters (ϕ_3, δ) and (ϕ_3, a) with systematic uncertainty included. The 90% confidence intervals for the fit parameters (including systematic uncertainty) are: $0.15 < a < 0.50$, $61^\circ < \phi_3 < 142^\circ$ and $104^\circ < \delta < 214^\circ$.

CONCLUSION

We have applied a new method to measure the CP-sensitive angle ϕ_3 using the Dalitz analysis of the three-body D^0 decay in the process $B \rightarrow D^0 K$. The method is directly sensitive to the value of ϕ_3 and is free from discrete ambiguities (for the ϕ_3 values in the range from 0 to 180°). The statistical and systematic uncertainties of this method were studied using MC simulation. The statistics of 1000 fb^{-1} should permit us to determine ϕ_3 with a 10° statistical uncertainty. We estimate the model uncertainty of the method to be of the order of 10° . This uncertainty can be significantly reduced with the increase of associated experimental data, and practically eliminated by using the data from the $c\tau$ -factory [3].

The first measurement of ϕ_3 using this technique was performed based on 140 fb^{-1} statistics collected by the Belle detector. The significance of the direct CP violation effect (including systematic effects) is 2.4 standard deviations. The values of ϕ_3 and relative amplitude a obtained are in agreement with the SM expectation. The 90% confidence interval obtained for the ϕ_3 value is $61^\circ < \phi_3 < 142^\circ$. The accuracy of the measurement can be improved in the future by adding other suitable decay modes into the analysis.

ACKNOWLEDGEMENTS

We wish to thank the KEKB accelerator group for the excellent operation of the KEKB accelerator. We acknowledge support from the Ministry of Education, Culture, Sports, Science, and Technology of Japan and the Japan Society for the Promotion of Science; the Australian Research Council and the Australian Department of Education, Science and Training; the National Science Foundation of China under contract No. 10175071; the Department of Science and Technology of India; the BK21 program of the Ministry of Education of Korea and the CHEP SRC program of the Korea Science and Engineering Foundation; the Polish State Committee for Scientific Research under contract No. 2P03B 01324; the Ministry of Science and Technology of the Russian Federation; the Ministry of Education, Science and Sport of the Republic of Slovenia; the National Science Council and the Ministry of Education of Taiwan; and the U.S. Department of Energy.

* on leave from Fermi National Accelerator Laboratory, Batavia, Illinois 60510

† on leave from University of Pittsburgh, Pittsburgh PA 15260

‡ on leave from Nova Gorica Polytechnic, Nova Gorica

- [1] M. Kobayashi and T. Maskawa, *Prog. Theor. Phys.* **49**, 652 (1973); N. Cabibbo, *Phys. Rev. Lett.* **10**, 531 (1963);
- [2] M. Gronau and D. Wyler, *Phys. Lett.* **B265**, 172 (1991); I. Dunietz, *Phys. Lett.* **B270**, 75 (1991); D. Atwood, G. Eilam, M. Gronau and A. Soni, *Phys. Lett.* **B341**, 372 (1995); D. Atwood, I. Dunietz and A. Soni, *Phys. Rev. Lett.* **78**, 3257 (1997).
- [3] A. Giri, Yu. Grossman, A. Soffer, J. Zupan, hep-ph/0303187.
- [4] CLEO Collaboration, M. Athanas *et al.*, *Phys. Rev. Lett.* **80**, 5493 (1998).
- [5] Belle Collaboration, P. Krokovny *et al.*, *Phys. Rev. Lett.* **90**, 141802 (2003).
- [6] Belle Collaboration, K. Abe *et al.*, *Phys. Rev. Lett.* **87**, 111801 (2001).
- [7] M. Gronau, *Phys. Lett. B* **557**, 198 (2003)
- [8] CLEO Collaboration, H. Muramatsu *et al.*, *Phys. Rev. Lett.* **89**, 251802 (2002), Erratum-ibid: **90**, 059901 (2003).
- [9] CLEO Collaboration, S. Kopp *et al.*, *Phys. Rev. D* **63**, 092001 (2001).
- [10] Belle Collaboration, A. Abashian *et al.*, *Nucl. Instr. and Meth. A* **479**, 117 (2002).
- [11] CLEO Collaboration, D. M. Asner *et al.*, *Phys. Rev. D* **53**, 1039 (1996)
- [12] ARGUS collaboration, H. Albrecht *et al.*, *Phys. Lett. B* **241**, 278 (1990).

TABLE I: List of resonances used for $\bar{D}^0 \rightarrow K_s \pi^+ \pi^-$ decay simulation.

Resonance	Amplitude	Phase, (deg)
$K^*(892)^+ \pi^-$	1.56	150
$K_s \rho^0$	$\equiv 1$	$\equiv 0$
$K^*(892)^- \pi^+$	0.11	321
$K_s \omega$	0.037	114
$K_s f_0(980)$	0.34	188
$K_s f_0(1370)$	1.8	85
$K_0^*(1430)^+ \pi^-$	2.0	3
$K_s \pi^+ \pi^-$ non-resonant	1.1	160

TABLE II: Estimation of ϕ_3 model systematics.

Fit model	$(\Delta\phi_3)_{max}$ (deg)
$K^*(892)$, ρ , nonres	29.3
$K^*(892)$, ρ , DCS $K^*(892)$, nonres	6.7
$K^*(892)$, ρ , DCS $K^*(892)$, $f^0(980)$, nonres	9.9
$F_r = F_D = 1$	3.1
$\Gamma(q^2) = Const$	4.7

TABLE III: Fit results for $D^0 \rightarrow K_s \pi^+ \pi^-$ decay. Errors are statistical only.

Resonance	Amplitude	Phase, (deg)
$K^*(892)^- \pi^+$	1.706 ± 0.015	138.0 ± 0.9
$K_s \rho^0$	1.0 (fixed)	0 (fixed)
$K^*(892)^+ \pi^-$	$(13.6 \pm 0.8) \times 10^{-2}$	330 ± 3
$K_s \omega$	$(32.8 \pm 1.8) \times 10^{-3}$	114 ± 3
$K_s f_0(980)$	0.385 ± 0.011	214.2 ± 2.3
$K_s f_0(1370)$	0.49 ± 0.04	311 ± 6
$K_s f_2(1270)$	1.66 ± 0.05	341.3 ± 2.3
$K_0^*(1430)^- \pi^+$	2.09 ± 0.05	353.6 ± 1.8
$K_2^*(1430)^- \pi^+$	1.20 ± 0.05	316.9 ± 2.1
$K^*(1680)^- \pi^+$	1.62 ± 0.24	84 ± 10
$K_s \sigma_1$ ($M_{\sigma_1} = 535 \pm 6$ MeV, $\Gamma_{\sigma_1} = 460 \pm 15$ MeV)	1.66 ± 0.09	217.3 ± 1.4
$K_s \sigma_2$ ($M_{\sigma_2} = 1063 \pm 7$ MeV, $\Gamma_{\sigma_2} = 101 \pm 12$ MeV)	0.31 ± 0.04	257 ± 11
non-resonant	6.51 ± 0.22	149.0 ± 1.6

TABLE IV: Estimation of systematic uncertainties.

Source	Δa	$\Delta\phi_3$, (deg)	$\Delta\delta$, (deg)
D^0 decay model	0.03	10	24
Background shape	0.015	3.2	2.3
Efficiency shape	0.010	2.4	0.8
Momentum resolution	0.010	2.5	0.6
Test sample bias	0.02	12	12
Total	0.04	16	27

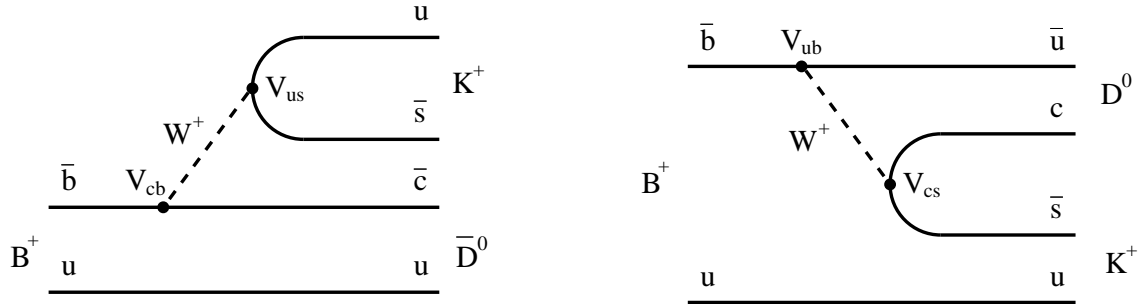


FIG. 1: Diagrams of $B^+ \rightarrow \bar{D}^0 K^+$ (left) and $B^+ \rightarrow D^0 K^+$ (right) decays.

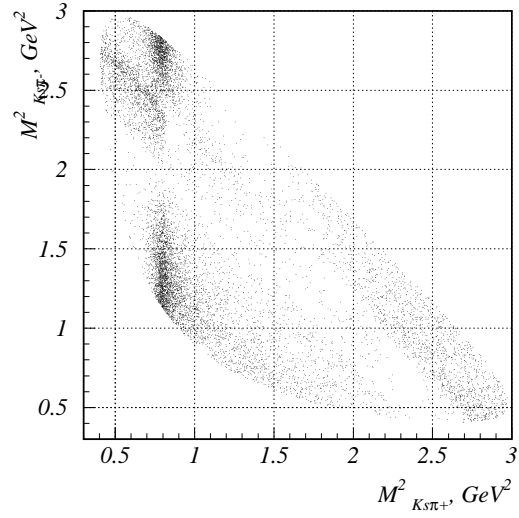


FIG. 2: Simulated Dalitz plot of $\bar{D}^0 \rightarrow K_s \pi^+ \pi^-$ decay.

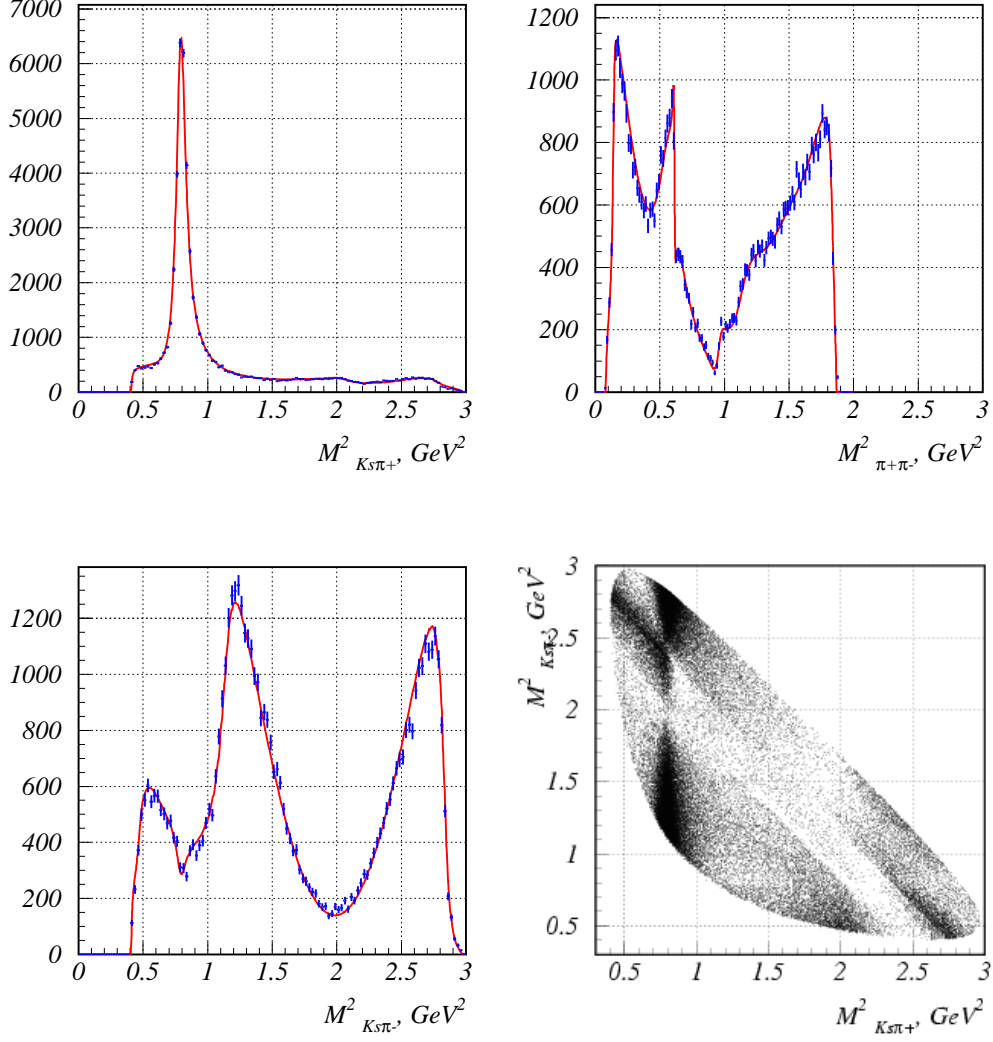


FIG. 3: $M^2_{K^+ \pi^+}$, $M^2_{K^+ \pi^-}$, $M^2_{\pi^+ \pi^-}$ distributions and Dalitz plot of $D^0 \rightarrow K_s \pi^+ \pi^-$ decay from $D^{*+} \rightarrow D^0 \pi$ process.

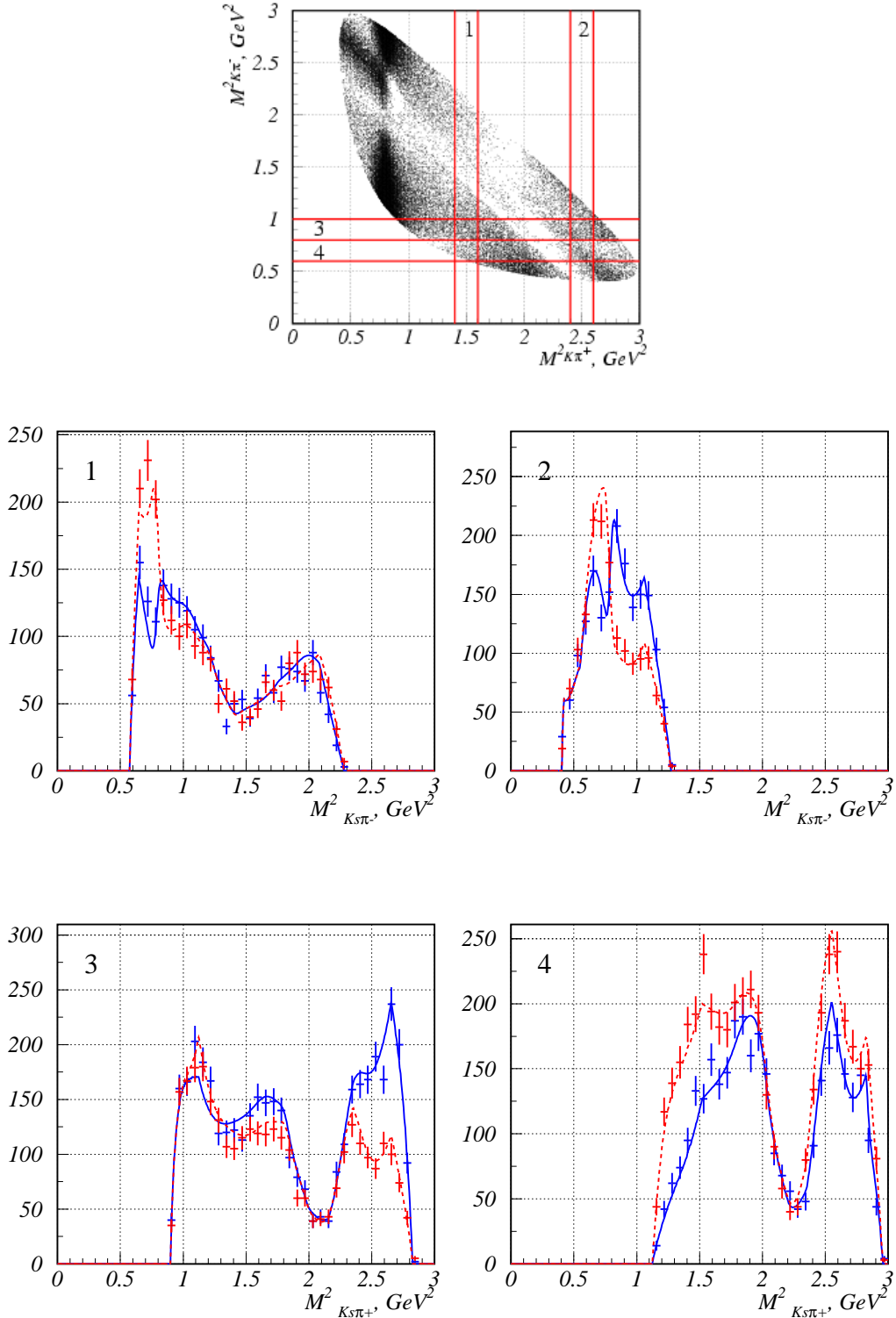


FIG. 4: Simulated Dalitz plot of D^0 decay and its slices showing the effect of CP asymmetry in $B \rightarrow D^0 K$ decay with the parameters $a = 0.125$, $\phi_3 = 70^\circ$ and $\delta = 0$. The two curves represent the Dalitz plot density for D^0 decay from $B^+ \rightarrow \bar{D}^0 K^+$ (solid line) and $B^- \rightarrow D^0 K^-$ (dashed line) processes.

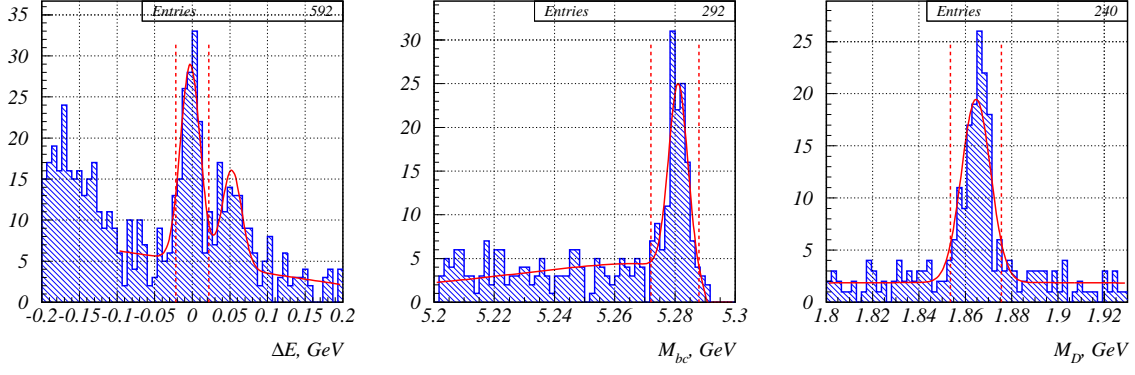


FIG. 5: ΔE , M_{bc} and M_D distributions for $B \rightarrow D^0 K$ decay. Histogram represents the data, the solid line is the fit result, dashed lines show the cut limits for the corresponding distributions.

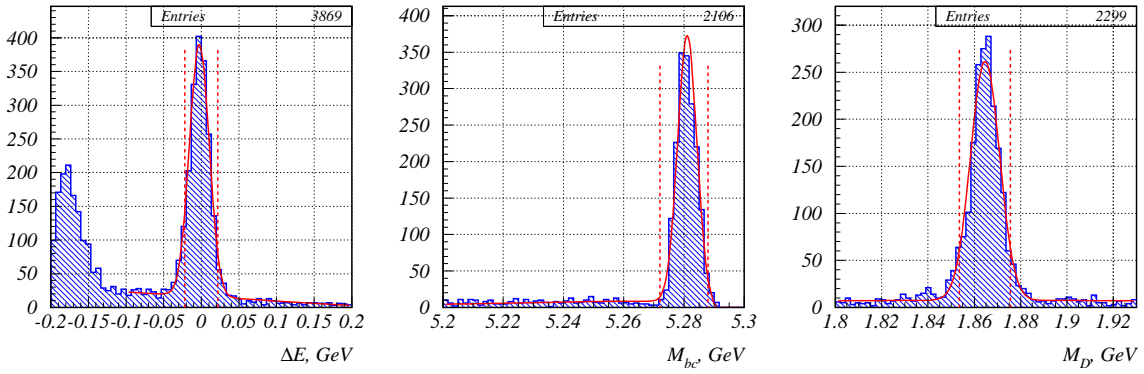


FIG. 6: ΔE , M_{bc} and M_D distributions for $B \rightarrow D^0 \pi$ decay.

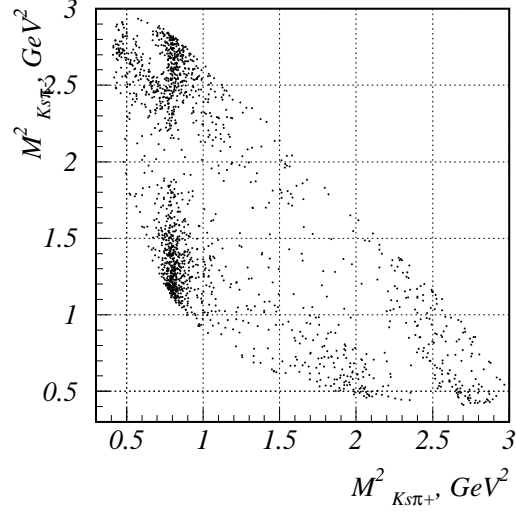


FIG. 7: Dalitz distribution in variables $m^2_{K_s\pi^+}$, $m^2_{K_s\pi^-}$ of $D^0 \rightarrow K_s\pi^+\pi^-$ decay from $B \rightarrow D^0\pi$ process.

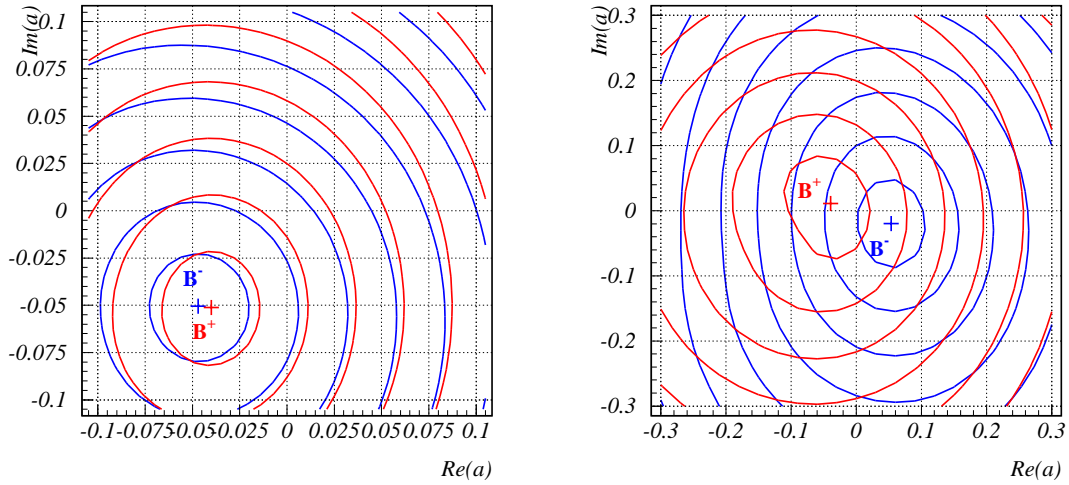


FIG. 8: Constraint plots of complex relative amplitude $ae^{i\theta}$ for $B \rightarrow D^0\pi$ (left) and $B \rightarrow D^{*0}\pi$ (right) decays. Contours indicate integer multiples of the standard deviation.

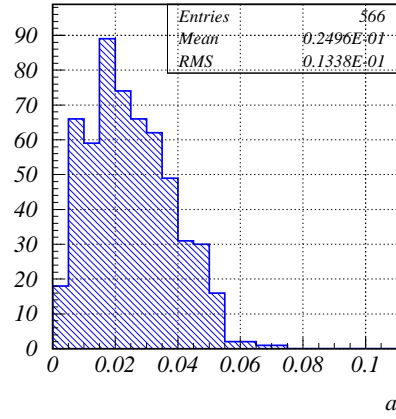


FIG. 9: Distribution of the fitted parameter a in 566 trials of 1700 events each, generated with $a = 0$.

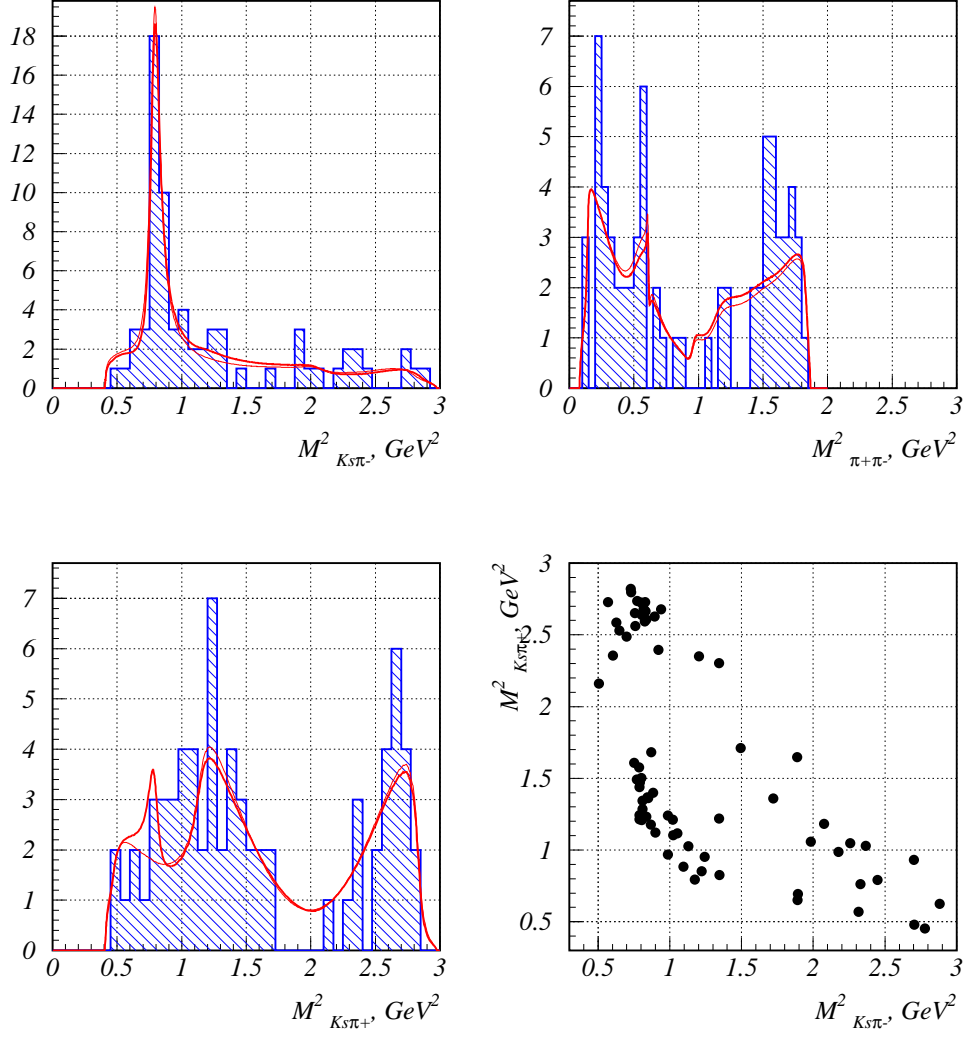


FIG. 10: $M_{K\pi^-}^2$, $M_{K\pi^+}^2$, $M_{\pi^+\pi^-}^2$ distributions and Dalitz plot of $D^0 \rightarrow K_s \pi^+ \pi^-$ decay from $B^- \rightarrow D^0 K^-$ process. Thick line represents the fit result, thin line is $a = 0$ case.

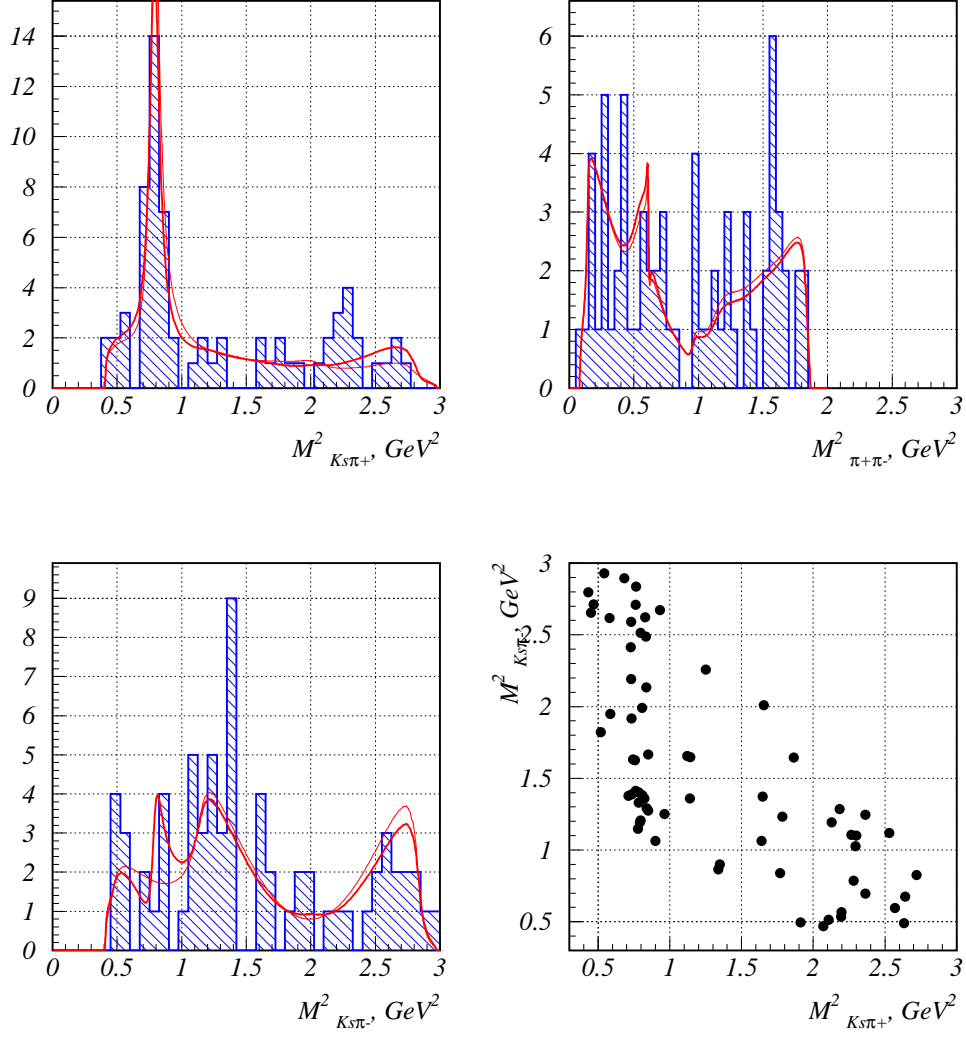


FIG. 11: $M^2_{K\pi^+}$, $M^2_{K\pi^-}$, $M^2_{\pi^+\pi^-}$ distributions and Dalitz plot of $D^0 \rightarrow K_s \pi^+ \pi^-$ decay from $B^+ \rightarrow \bar{D}^0 K^+$ process. Thick line represents the fit result, thin line is $a = 0$ case.

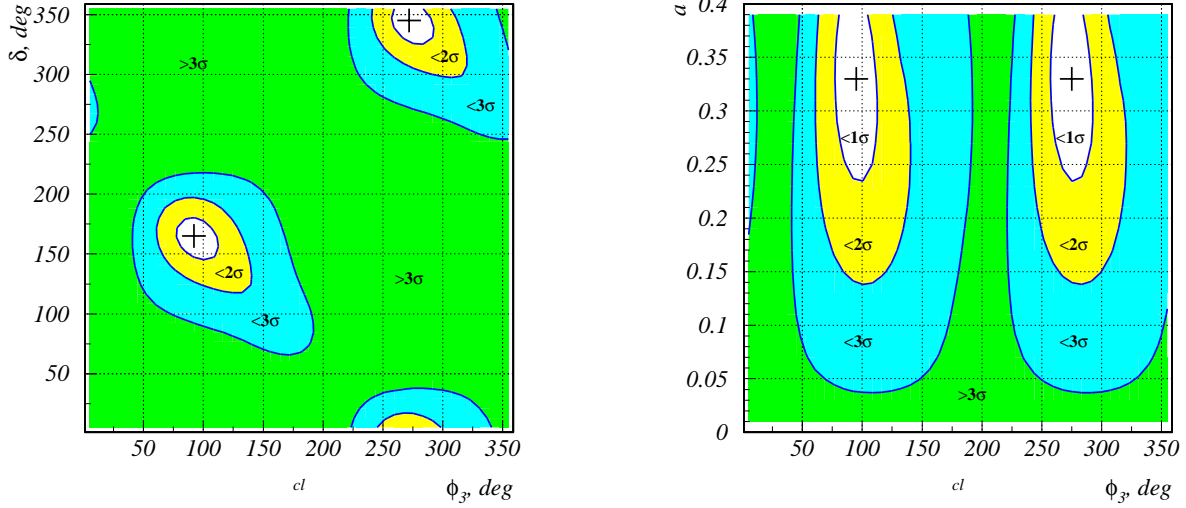


FIG. 12: Constraints on ϕ_3 and δ (left) and a and ϕ_3 (right) for all parameters free in the fit.

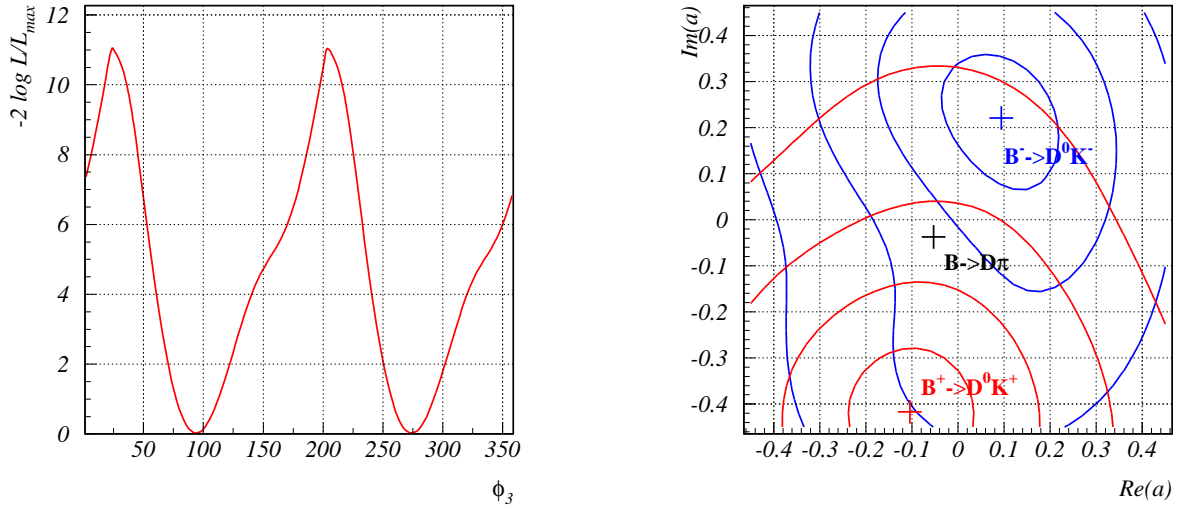


FIG. 13: ϕ_3 statistical significance (left) and results of the complex relative amplitude $a \exp(i\theta)$ fits for $B^+ \rightarrow \bar{D}^0 \pi^+$ and $B^- \rightarrow D^0 \pi^-$ samples (right). Contours indicate integer multiples of the standard deviation.

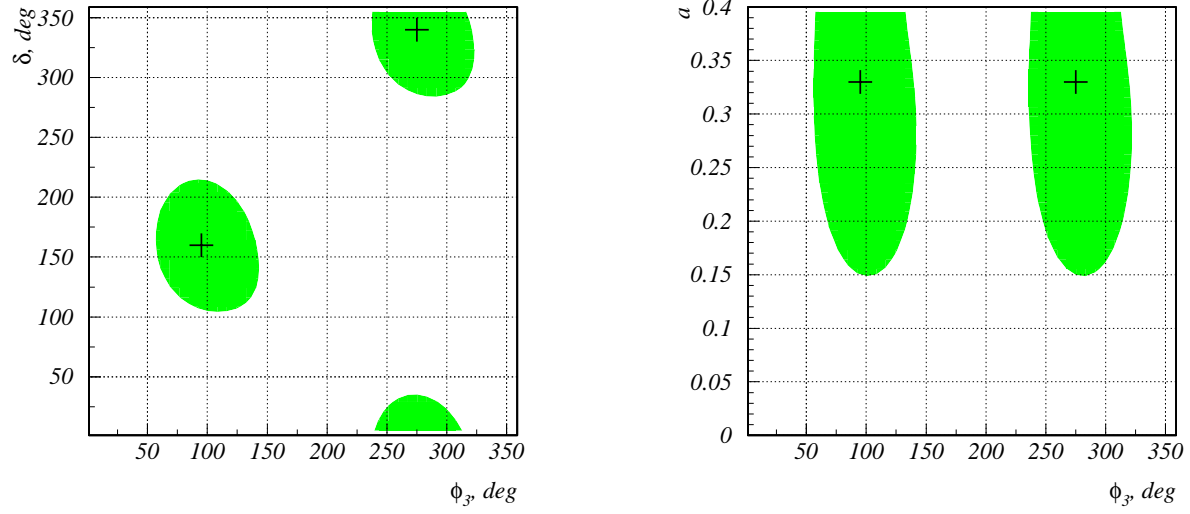


FIG. 14: 90% CL regions for ϕ_3 and δ (left) and a and ϕ_3 (right) with systematic uncertainty included.